Acta of Bioengineering and Biomechanics
Vol. 25, No. 3, 2023

Original paper
DOI: 10.37190/ABB-02264-2023-04

Tensile and flexural moduli for human orbital wall bones – comparative study

PAWEŁ LEMSKI[1], KRZYSZTOF ŻERDZICKI[2]*, PAWEŁ KŁOSOWSKI[2], ANDRZEJ SKOREK[1, 3], MARCIN ADAM ŻMUDA TRZEBIATOWSKI[2]

[1] Department of Otolaryngology, Copernicus Hospital, Gdańsk, Poland.
[2] Faculty of Civil and Environmental Engineering, Gdańsk University of Technology, Gdańsk, Poland.
[3] Medical Department, Academy of Applied Medical and Social Sciences, Elbląg, Poland.

The main aims of the current research were: (1) to analyze in detail the tensile modulus and ultimate tensile strength (UTS) of orbital wall bones separately for the left and right orbit of the same cadaver and (2) to compare the obtained results with a flexural modulus of the left and right orbit reported earlier by A. C. van Leeuwen et al. [14].

A set of 54 specimens of orbital superior and/or medial walls harvested from 16 human skulls (4 female, 12 male) were tensioned at 0.01 mm/s till fracture. The samples were taken always from both orbits of the same cadaver. For each sample, cross-section area, apparent density, tensile modulus, and UTS were identified.

For pooled female and male group apparent density for right and left orbit was identified to be 1.59 (± 0.52 SD) g/cm^3 and 1.51 (±0.48 SD) g/cm^3, tensile modulus of 2028 (±1729 SD) MPa and of 2706 (±2812 SD) MPa, and UTS of 14.17 (±15.00 SD) MPa and of 15.03 (±11.44 SD) MPa, respectively. For tensile tests, there were no statistical differences between the left and right orbit for pooled male and female groups for (a) apparent density (Student's *t*-test $p = 0.567$), (b) UTS (Mann–Whitney *U*-test $p = 0.350$) and (c) tensile modulus (Mann–Whitney *U*-test $p = 0.716$). For bending tests, there were no statistical differences between the left and right orbit for the pooled male and female group for (a) orbital wall thickness (Student's *t*-test $p = 0.811$) and (b) flexural modulus (Mann–Whitney *U*-test $p = 0.206$). The comparative analysis between tensile and flexural moduli for pooled left and right groups (with no distinction for male and female) revealed no statistically significant difference (Mann–Whitney *U*-test $p = 0.074$). The maximum tensile modulus was 7279 MPa and 9913 MPa for the right and left orbit, respectively, and was similar to the maximum flexural modulus of 6870 MPa and 9170 MPa reported in an earlier study, for the right and left orbit, respectively.

Key words: *orbital wall bone, laboratory experiments, tensile modulus, flexural modulus, identification*

1. Introduction

For an anatomical reconstruction of the injured orbital wall, a wide range of different materials is used: biological materials (including autogenous materials, allografts or animal-derived materials), metals (especially titanium and cobalt alloys), polymers (polyethene, silicon, nylon, polylactic acid – PLA, polyglycolic acid – PGA, Polydioxanone – PDS) and composites (like, eg., Titanium/PE, PLA-based polymer sheet, Bone marrow-coated PCL scaffolds, etc.). Application of the appropriate implant materials improves patient treatment considerably [6]. The principal role of the implant is to support the orbital content and to restore the orbit contour, especially in larger fractures, thus preserving from the occurrence of enophthalmos and hypoglobus [8], [25]. Therefore, during the reconstruction of the orbital floor, it is of the highest importance to identify a stable zone of bone where the bone graft or the implant can be securely anchored [19]. For patient safety and to avoid additional complicated surgeries, medical

* Corresponding author: Krzysztof Żerdzicki, Faculty of Civil and Environmental Engineering, Gdańsk University of Technology, ul. Narutowicza 11/12, 80-233 Gdańsk, Poland, e-mail: krzysztof.zerdzicki@pg.edu.pl (K. Żerdzicki).
Received: June 2nd, 2023
Accepted for publication: October 31th, 2023

treatment in orbital zone injuries is more often preceded by numerical calculations based on the patient individual skull model [9], [13]. For instance, due to the blowout trauma, the type of fracture of the orbit bone depends on the mechanism of the orbit loading, which means the tensile loading character for the hydraulic mechanism and bending/compression loading for the buckling mechanism [18]. This issue was comprehensively studied through numerical modeling and clinical observations, and was reported before [27], [28]. For a comprehensive understanding of the mechanics and strength of the orbital wall bones and thus easier manufacturing of the implant or better selection of reconstruction technic, research on mechanical properties of the orbital wall bones is still required. However, the study toward Young's modulus identification is difficult, as the experiments are conducted on non-standardized samples due to large anatomic variations in bone thickness, geometry, and the presence of paranasal sinuses in the craniofacial zone [7]. To omit this problem, it is valuable to conduct and report more research including bending and tensile properties of the orbital wall bones. Only the independent, properly planned and direct experimental strength tests is able to throw light on the real mechanical properties of the interior bones of the human head. The mechanical properties (elastic tensile and bending) of the orbital walls are evidently different from the well-known mechanical properties of long bones or skull outside bones (such as mandibular or maxilla bone, parietal and occipital bones, etc.). Due to its small thickness and in-plane size, the orbital wall bones are difficult to extract for mechanical tests.

The current study aims at providing quantitative data on tensile properties identified for orbital wall bones, thus improving numerical models for adult patients with orbital zone fractures and helping with the selection of the best implant to be used during the anatomical reconstruction of the fractured orbital zone.

2. Materials and methods

2.1. Sample preparation

Results presented hereby are a part of a larger research carried out before by Żerdzicki et al. [26], where focus was put on the mechanical differences between properties identified for the specimens cut in coronal and sagittal planes. Here, we compare in detail the tensile properties between the left and right orbit only to enable direct comparison with the similar procedure done by A.C. van Leeuwen et al. [14] for bending tests.

The research was carried out after acceptance from the Independent Bioethics Committee and was performed according to Declaration of Helsinki [1] and the European Union's Directive 2004/23/WE art. 13,15 [23]. Informed consent to use the clinical data was obtained from the family, when possible. The biological material was harvested from 16 cadavers (aged between 35 to 75 years old, 12 male and 4 female). The samples were collected exclusively from patients without any chronic diseases or head injuries and a history indicating pathological fractures, which may have been caused by osteoporosis. The whole orbital wall blocks were collected from cadavers no later than 2–5 days after their death. Specimen blocks were kept hydrated in the 0.9 NaCl solution and frosted at –20 °C for a maximum of 36 hours before testing. Then, the samples were defrosted for about 12 hours at room temperature before measurements and mechanical testing. They were gently placed in a specially prepared container, without direct contact with other items and heat sources such as sunlight or heaters to prevent their damage and avoid changing their properties. The sample preparation method was comparable to the procedure proposed by Morgan et al. [16] for mechanical experiments on human vertebra, tibia, and femur.

After defrosting, the specimens were cut out from the superior and medial walls of the orbit. As many as possible bone samples were prepared from one orbit (minimum 1, maximum 3), thus, the final count of the specimens tested was 54. The final specimens had approximately the following dimensions: 7–15 mm wide, 0.7–2.3 mm thick and, 30–40 mm long. There was also a principal rule, that from the left orbit, only samples in the coronal direction were cut and from the right orbit, only samples cut along the sagittal plane were prepared. Then, the apparent density of every specimen was obtained based on the Archimedes principle. The samples were weighed in the dry state with an accuracy of 0.01 G, and their volume was determined by immersing the samples into water and basing them on the change in water level in the measuring glass with an accuracy of 1 ml. The time of immersion was as short as possible, and then the samples were surface-dried with a paper towel and were tested almost immediately.

For the study regarding bending tests upon orbital wall bones [14], two samples were collected from every of 14 fresh-frozen cadaveric heads (12 male and 3 female, aged 70 ± 8.3 years), therefore, the total

number of samples was 28. The samples were cut from the medial part of the orbital floor, the medial of the infraorbital nerve, and the lateral of the medial wall [14]. The reported value of flexural modulus was taken for each patient and with distinction for left and right orbit (Table 3 in [14]).

2.2. Mechanical testing

The tests were conducted using the Zwick/Roell Z020 testing machine (Fig. 1). Dedicated machine grips for asymmetric, non-linear-shaped samples were used for the steady fixation of bone fragments at a testing machine. The preload of 10 N was applied, and then the samples were uniaxial tensioned till fracture with 0.01 mm/s crosshead speed. During the test, the elongation of the sample was precisely measured by the video extensometer that tracked white markers put on each sample in the central zone of the bone fragment (Fig. 2). The changes of force and elongation were recorded with 10 Hz frequency by TestXpert software of the Zwick/Roell testing stand. No slippage of the samples was observed during the loading. The specimen behavior was almost purely elastic till the fracture, only small plastic effects were noticed. The samples are usually fractured in the middle part of the specimen. The sample did not split into two regular parts, rather the failure had a local character. Right after the sample failure, the specimen was cut in half near the fracture line and the cross-section of both obtained parts was imprinted with ink on the plain not-absorbable fabric material (Fig. 3). Next, the photographs of the imprints close to a ruler were taken and imported to the AutoCAD software to calculate the cross-section area according to the scale given. In Table 1, the mean cross-section area of the left and right imprints of the same specimen is reported for every specimen included in the study.

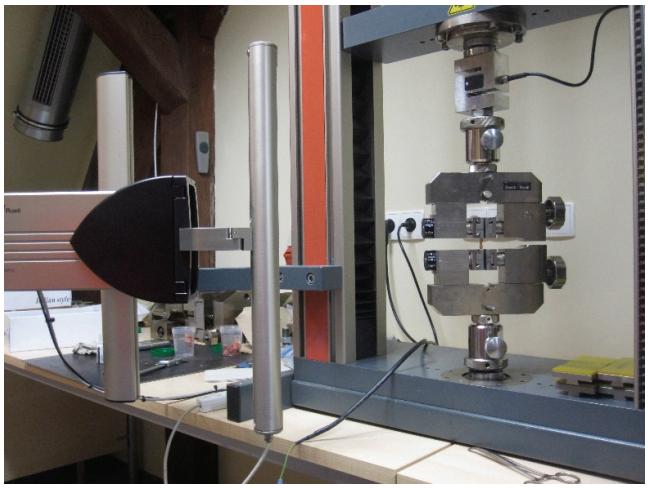

Fig. 1. Experimental stand with the video-extensometer

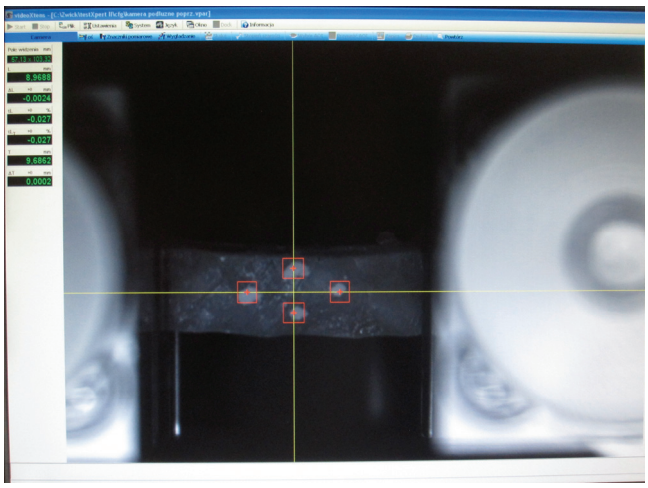

Fig. 2. Video extensometer view on human orbital wall bone sample placed in Zwick Roell Z020 testing machine. Displacement of white markers used for elongation calculation

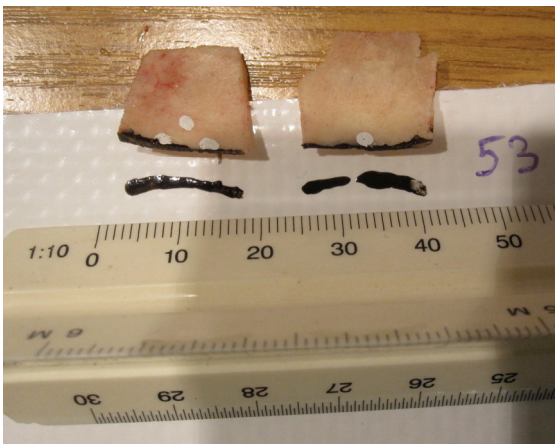

Fig. 3. Orbital wall sample cut in the middle and cross-section of both parts outlined by ink for cross-section area evaluation by AutoCAD software (scale specified by millimetre ruler)

2.3. Elastic tensile modulus identification

Firstly, having the force, cross-section area, and elongation change between extensometer markers, the stress and strain values were calculated using the standard formulas. Then, the stress-strain curves were prepared and its beginning linear part up to 0.5% of total strain was approximated by a linear function using the least squares method (Fig. 4). The elastic tensile modulus (usually called Young's modulus) was defined as the slope of the approximation line. The ultimate tensile stress (UTS) was specified as the

greatest stress value registered before the fracture of the sample. The mean value of the particular parameter was calculated for each patient separately with distinction for left and right orbit, as it was reported in the same manner in the previous research [14].

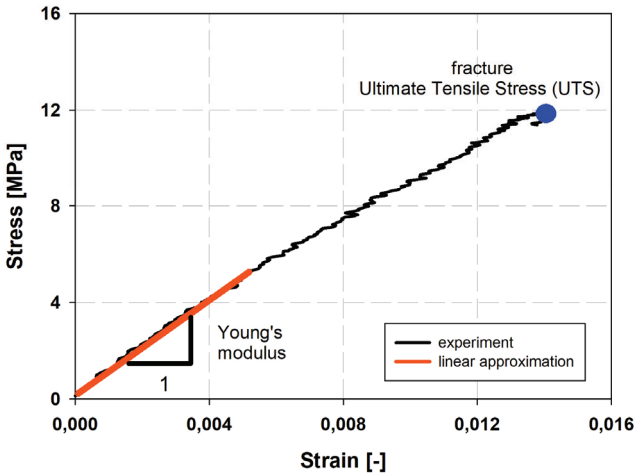

Fig. 4. Exemplary stress–strain graph with parameters analyzed

2.4. Statistical evaluation

The statistics of the results acquired in the current research and reported in [14] were realized in SigmaPlot 12.5 software. For both studies separately, the results for female and male specimens were pooled together and divided into left and right orbit groups. As the number of female samples was smaller than the male ones it was pointless to divide the results additionally into female and male groups. The Shapiro–Wilk test was used to assess the normal distribution of the relevant parameters. The Student's *t*-test was used to individually compare groups with normal distribution, while the Mann–Whitney *U*-test was used for the individual comparisons between groups with non-normal distribution.

3. Results

The bone tissue material was collected from 16 different cadavers (aged between 35 to 75 years old, mean age 56.7 ± 9.9 years old, 14 males and 2 females) in the current study and from 14 different cadavers (aged between 55 to 79 years old, mean age 70.4 ± 8.4 years old, 12 males and 2 females) in the previously reported research [14]. The results from the current study including sample mean cross-section area, tensile modulus, and UTS values exhibited non-parametric distribution, therefore minimum, maximum, median, and interquartile range (IQR) values of the parameters are presented in Table 1. The outcomes of the flexural modulus and thickness of the samples tested are presented in Table 3 in [14]. The flexural modulus values also exhibited non-parametric distribution with a median of 2555 MPa and IQR of 1260–4550 MPa [14].

The comparative analysis of the elastic modulus obtained from uniaxial tensile tests and three-point bending tests is enclosed in Table 2. For tensile tests, there were no statistical differences between the left and right orbit for pooled male and female groups for (a) apparent density (Student's *t*-test $p = 0.567$), (b) UTS (Mann–Whitney *U*-test $p = 0.350$) and (c) tensile modulus (Mann–Whitney *U*-test $p = 0.716$). For bending tests, there were no statistical differences between the left and right orbit for the pooled male and female

Table 1. Identification results of all specimens included in the current study [26]

Specimen	Sex	Age [years]	Side	Average cross-section area [mm^2]	Density [g/cm^3]	Density mean for side [g/cm^3]	UTS [MPa]	UTS mean for side [MPa]	Tensile modulus [MPa]	Tensile modulus mean for side [MPa]
1	**2**	**3**	**4**	**5**	**6**	**7**	**8**	**9**	**10**	**11**
1	M	62	right	10.8	1.66	1.34	2.99	4.26	1617	1574
			right	25.5	1.42		5.36		1899	
			right	19.8	0.95		4.42		1206	
			left	28.2	1.60	1.45	5.95	6.40	1109	3708
			left	12.9	1.30		6.85		6307	
2	M	60	right	14.9	2.00	1.53	26.74	19.03	2982	3309
			right	22.0	1.07		11.32		335	
			left	23.3	1.42	1.29	17.80	10.65	5072	3362
			left	31.3	1.15		3.51		1651	

1	2	3	4	5	6	7	8	9	10	11
3	M	49	right	18.1	1.28	1.41	4.72	5.22	1452	1754
			right	28.0	1.55		5.71		2057	
			left	26.7	1.49	1.41	17.00	15.07	1555	1507
			left	48.6	1.33		13.14		1459	
4	M	49	right	31.0	1.69	1.69	2.83	2.83	363	364
			left	27.5	1.52	1.60	8.81	4.98	455	498
			left	59.1	1.68		1.14		541	
5	M	42	right	11.2	2.32	2.32	6.75	6.75	298	298
			left	41.5	1.75	1.65	20.83	25.25	2193	4301
			left	33.7	1.56		29.68		6408	
6	M	35	right	13.2	1.48	1.49	24.90	37.35	4978	4097
			right	13.8	1.50		49.80		3216	
			left	12.4	1.50	1.60	32.16	28.34	9913	5481
			left	4.4	1.71		24.52		1049	
7	M	54	right	23.6	1.91	1.75	14.47	12.92	983	2002
			right	9.1	1.60		11.37		3020	
			left	31.2	1.47	1.43	16.12	16.37	5634	4068
			left	27.5	1.40		16.62		25021	
8	M	59	right	30.8	2.00	2.00	11.88	11.88	829	829
			left	16.5	2.04	2.04	40.77	40.77	8962	8962
9	M	75	right	12.4	2.18	2.18	4.65	4.65	875	875
			left	29.4	1.30	1.49	5.16	6.77	1042	1065
			left	13.7	1.68		8.37		1087	
10	M	50	right	22.2	1.44	1.82	32.72	30.94	7279	5154
			right	19.0	2.20		29.16		3030	
			left	19.4	0.59	0.59	26.90	26.90	2700	2700
11	M	64	right	52.2	2.09	2.09	5.00	5.00	888	888
			left	53.5	2.98	2.98	7.50	7.50	2061	2061
12	F	62	right	17.0	0.66	0.86	2.79	2.41	343	618
			right	16.6	1.06		2.02		893	
			left	20.5	1.42	1.30	1.70	1.84	812	532
			left	22.7	1.19		1.96		252	
13	F	54	right	16.3	2.20	2.20	1.12	1.12	996	996
			left	33.9	2.00	2.00	0.43	0.43	114	114
14	F	66	right	13.3	0.62	0.62	60.02	60.02	5444	5444
			left	23.0	1.71	1.95	34.60	32.36	3131	4759
			left	21.3	2.20		30.11		6386	
15	F	64	right	25.7	1.87	1.63	5.04	5.24	2378	2135
			right	45.0	1.39		5.44		1891	
			left	22.1	1.42	1.25	7.63	11.15	216	270
			left	20.5	1.08		14.67		325	
16	F	63	right	9.8	2.00	1.63	27.02	17.11	1032	737
			right	27.5	2.26		8.98		976	
			right	13.4	0.62		15.34		204	
			left	12.7	0.40	0.40	11.78	11.78	126	126
		60 ± 10			1.55 ± 0.50 median 1.51 IQR 1.30 –1.93		median 10.15 IQR 4.93 –24.62		median 1507 IQR 863 – 3055	

group for (a) orbital wall thickness (Student's *t*-test $p = 0.811$) and (b) flexural modulus (Mann–Whitney *U*-test $p = 0.206$). The comparative analysis between tensile and flexural moduli for pooled left and right groups (with no distinction for male and female) revealed no statistically significant difference (Mann–Whitney *U*-test $p = 0.074$). There were only two samples with flexural moduli identified for females, thus it was not possible to perform comparisons between genders.

The minimum values for left and right orbit are much lower for tensile modulus (115 MPa and 204 MPa, respectively) than for flexural moduli (790 MPa and 670 MPa, respectively), but the maximum values for tensile modulus (9913 MPa and 7279 MPa, respectively) and flexural modulus: (6870 MPa and 9170 MPa,

Table 2. Comparison between flexural [14] and tensile modulus (current study) for the left and right human orbit

Parameter	Flexural modulus [1] [MPa]			Tensile modulus [MPa]		
	Left	Right	Pooled (left + right)	Left	Right	Pooled (left + right)
Minimum	670	790	670	115	204	115
Maximum	9170	6870	9170	9913	7279	9913
Median	2180	3185	2555	1555	1452	1507
IQR	775–3850	1980–4660	1260–4550	540–5072	888–3019	863–3055

respectively) are very similar. The median for the left and right sides is almost identical for the tensile modulus (1555 MPa and 1452 MPa, respectively), while for the flexural modulus, the dispersion is much higher (3185 MPa and 2555 MPa, respectively).

4. Discussion

Floor and medial orbital wall zones remain the most common locations of all orbital fractures [2], [5]. For a reconstruction of the fracture, a computer-assisted approach including patient-specific anatomical modeling and custom-made implant fabrication is still being developed to produce the individually ideal implant in regards to geometry and material parameters [4]. Computer-aided design (CAD), computer-aided manufacturing (CAM), and computer-aided analysis (CAE) technologies already demonstrated significant advantages in implant reconstruction of facial and cranial bones [3], [4]. It allows not only for the design and manufacturing of the final implant by 3D printing [10] or mould performed [3] technology but also for precise evaluation of the injury pattern with its range and exact measurements of the orbital volume and its pathological or induced changes [4], [27]. One of the most often performed is the finite element (FE) modeling which is willingly used for biomechanical analysis of different head region traumas. Numerical modeling always requires geometry, which is usually taken from computer tomography, and material properties of the implant and human tissues where the implant is to be anchored. When it comes to the surgery technic, it is also stated that improvement of endoscopic sinus and skull base surgery (ESSBS) with virtual reality simulators (VRS) is to be based on the biomechanical research on skull base tissue [7], where the orbital wall bone need special attention. This technique involves hepatic feedback which is a powerful tool [11] but still needs more data, especially the Young's modulus of the human tissues to work properly during surgery.

There are several studies concerning the mechanical properties of the human head, where different testing approaches were implemented, including static bending tests [24], dynamic bending tests [2], [17], as well as indentation [15], nanoindentation and μCT measurements [17]. However, these studies were limited to the facial [21] and cranial [2], [17], [24] bones only. For numerical calculations of the inner bones of a human head usually, the approximated properties of the outer bones are taken [18] or the parameters obtained by Hounsfield unit recalculation based on CT scans of the human skull [20]. The authors of the current study are involved in the comprehensive analysis of the blowout trauma and accompanying fracture mechanisms, therefore they started extended numerical simulations and some preliminary laboratory testing toward mechanical properties of the human orbital wall bones [27], [28]. Appropriate modeling of the eyeball is an inseparable and very sophisticated aspect of the orbit region traumas [12], [22] as well.

To develop the state of the art and for a better understanding of the orbital zone biomechanics, the current paper provides new results on the tensile modulus of orbital wall bones and compares the results concerning elastic modulus identified in two different ways, based on uniaxial tensile tests and three-point bending tests [14]. The results of flexural and tension moduli are very close when comparing values of maximum moduli and very comparable in the IQR values, which confirms the correctness of the performed laboratory experiments and tensile modulus identification.

The presented results of apparent density, wall thickness, tensile modulus, flexural modulus, and UTS show no statistical dependency on the side of the human head and the sex of patients.

Among the limitations of the current study, the difficulty of getting a regular and repetitive shape of the finally tested samples should be mentioned. However, it is impossible to get better samples from the human orbital zone due to its irregular, curved shape according to the complicated anatomy of this region. Next, the diversification of results due to age was also omitted,

as most of the patients were above 50 years old and it was not possible to get samples from younger donors. Another drawback was the application of only four markers followed by a video-extensometer for specimen deformation analysis, instead of a more comprehensive DIC method. Unfortunately, the experimental laboratory was not equipped with a DIC system at the time of this research. The comparative analysis between tensile and bending properties of the orbital wall bones could be also more comprehensive, however, this kind of experiment is very rare, and studies regarding the bending mechanical tests are not widely reported.

Upon the assumption that the flexural and tensile modulus should be similar in the range of small deformations, the obtained from the current research study results of the tensile modulus can be used for the calculation of the implant based on the mathematical model presented in [14]. It is of the greatest importance to continue numerical modeling and computer simulations of the orbital wall region injuries, as the consensus of the best technique for repairing the medial wall fractures has not been achieved yet.

Acknowledgements

The financial support for the research by the National Science Center (NCN) in Kraków, Poland, within grant No. 016/23/B/ST8/00115 "*Analysis of the mechanical properties of the eye orbital wall and the numerical nonlinear dynamic analysis of the orbital blow-out trauma type verified by clinical observations"* is lawfully acknowledged.

Conflict of interests

The authors declare that there is no conflict of interest regarding the presented research.

References

[1] Association W M, *World Medical Association declaration of Helsinki: Ethical principles for medical research involving human subjects*, JAMA – J. Am. Med. Assoc., 310, 2191–2194.

[2] Auperrin A., Delille R., Lesueur D., Bruyère K., Masson C., Drazétic P., *Geometrical and material parameters to assess the macroscopic mechanical behaviour of fresh cranial bone samples*, J. Biomech., 2014, 47, 1180–1185.

[3] Brunzinii A., Mandolinii M., Manierii S., Gennanii M., Mazzoli A., Pagnoni M., Iannetti G., Modugn A., *Orbital wall reconstruction by selective laser sintered mould*, 2017, 260–264.

[4] Chepurnyi Y., Chernogorskyi D., Petrenko O., Kopchak A., *Reconstruction of Post-Traumatic Orbital Defects and Deformities with Custom-Made Patient-Specific Implants: Evaluation of the Efficacy and Clinical Outcome*, Craniomaxillofacial Trauma Reconstr. Open, 2019, 3, 0039–1685505.

[5] Chiang E., Saadat L.V., Spitz J.A., Bryar P.J., Chambers C.B., *Etiology of orbital fractures at a level I trauma center in a large metropolitan city*, Taiwan J. Ophthalmol., 2016, 6, 26–31.

[6] Chou C., Kuo Y.R., Chen C.C., Lai C.S., Lin S.D., Huang S.H., Lee S.S., *Medial orbital wall reconstruction with porous polyethylene by using a transconjunctival approach with a caruncular extension*, Ann. Plast. Surg., 2017, 78, S89–S94.

[7] Favier V., Gallet P., Subsol G., Captier G., *Understanding the biomechanical properties of skull base tissues is essential for the future of virtual reality endoscopic sinus and skull base surgery simulators*, Clin. Exp. Otorhinolaryngol., 2019, 12, 231–232.

[8] Gunarajah D.R., Samman N., *Biomaterials for repair of orbital floor blowout fractures: A systematic review*, J Oral Maxillofac. Surg., 2013, 71, 550–570.

[9] Heo J.J., Chong J.-H., Han J.J., Jung S., Kook M.-S., Oh H.-K., Park H.-J., *Reconstruction of the orbital wall using superior orbital rim osteotomy in a patient with a superior orbital wall fracture*, Maxillofac. Plast. Reconstr. Surg., 2018, 40, 1–5.

[10] Kang S., Kwon J., Ahn C.J., Esmaeli B., Kim G.B., Kim N., Sa H.S., *Generation of customized orbital implant templates using 3-dimensional printing for orbital wall reconstruction*, Eye, 2018, 32, 1864–1870.

[11] Kim D.H., Kim Y., Park J.S., Kim S.W., *Virtual reality simulators for endoscopic sinus and skull base surgery: The present and future*, Clin. Exp. Otorhinolaryngol., 2019, 12, 12–17.

[12] Koberda M., Skorek A., Kłosowski P., Żmuda Trzebiatowski M.A., Żerdzicki K., Lemski P., Stodolska-Koberda U., *Numerical and Clinical Analysis of an Eyeball Injuries Under Direct Impact*, Int. J. Occup. Med. Environ. Health, 2023, 36, 263–273.

[13] Larysz D., Wolański W., Kawlewska E., Mandera M., Gzik M., *Biomechanical aspects of preoperative planning of skull correction in children with craniosynostosis*, Acta Bioeng. Biomech., 2012, 14, 19–26.

[14] van Leeuwen A.C., Ong S.H., Vissink A., Grijpma D.W., Bos R.R.M., *Reconstruction of orbital wall defects: Recommendations based on a mathematical model*, Exp. Eye Res., 2012, 97, 10–18.

[15] Mazumder M.M.G., Miller K., Bunt S., Mostayed A., Joldes G., Day R., Hart R., Wittek A., *Mechanical properties of the brain-skull interface*, Acta Bioeng. Biomech., 2013, 15, 3–11.

[16] Morgan E.F., Bayraktar H.H., Keaveny T.M., *Trabecular bone modulus-density relationships depend on anatomic site*, J. Biomech., 2003, 36, 897–904.

[17] Motherway J.A., Verschueren P., Van der Perre G., Van der Sloten J., Gilchrist M.D., *The mechanical properties of cranial bone: The effect of loading rate and cranial sampling position*, J. Biomech., 2009, 42, 2129–2135.

[18] Nagasao T., Miyamoto J., Shimizu Y., Jiang H., Nakajima T., *What happens between pure hydraulic and buckling mechanisms of blowout fractures?*, J. Cranio-Maxillofacial. Surg., 2010, 38, 306–313.

[19] Reiter M.J., Schwope R.B., Theler J.M., *Postoperative CT of the orbital skeleton after trauma: Review of normal appearances and common complications*, Am. J. Roentgenol., 2016, 206, 1276–1285.

[20] Schaller A., Huempfner-Hierl H., Hemprich A., Hierl T., *Biomechanical mechanisms of orbital wall fractures – A tran-*

sient finite element analysis, J. Cranio-Maxillofacial. Surg., 2013, 41, 710–717.

[21] SEONG W.J., KIM U.K., SWIFT J.Q., HEO Y.C., HODGES J.S., KO C.C., *Elastic properties and apparent density of human edentulous maxilla and mandible*, Int. J. Oral Maxillofac. Surg., 2009, 38, 1088–1093.

[22] ŚRÓDKA W., *Effect of kinematic boundary conditions on optical and biomechanical behaviour of eyeball model*, Acta Bioeng. Biomech., 2006, 8, 69–77.

[23] Union Tep and the C of the E, Directive 2004/23/Ec of the European Parliament and of the Council of 31 March 2004 on setting standards of quality and safety for the donation, procurement, testing, processing, preservation, storage and distribution of human tissues and cells, Off. J. Eur. Union, 2004, 48–58.

[24] VERSCHUEREN P., DELYE H., BERCKMANS D., VERPOEST I., GOFFIN J., VAN DER SLOTEN J., VAN DER PERRE G., *Analysis of fracture characteristics of cranial bone for Fe modelling*, Int. Res. Counc. Biomech. Impact – 2006 Int. IRCOBI Conf. Biomech. Impact, Proc., 2006, 357–360.

[25] YE L.-X., SUN X.-M., ZHANG Y.-G., ZHANG Y., *Materials to facilitate orbital reconstruction and soft tissue filling in post-traumatic orbital deformaties*, Plast. Aesthetic Res., 2016, 3, 86.

[26] ŻERDZICKI K., LEMSKI P., KŁOSOWSKI P., SKOREK A., ŻMUDA TRZEBIATOWSKI M.A., KOBERDA M., *Tensile modulus of human orbital wall bones cut in sagittal and coronal planes*, PLoS One, 2021, 16, 1–15.

[27] ŻMUDA TRZEBIATOWSKI M.A., KŁOSOWSKI P., SKOREK A., ŻERDZICKI K., LEMSKI P., KOBERDA M., *Nonlinear dynamic analysis of the pure "buckling" mechanism during blow-out trauma of the human orbit*, Sci. Rep., 2020, 10, 1–13.

[28] ŻMUDA TRZEBIATOWSKI M.A., KŁOSOWSKI P., SKOREK A., ŻERDZICKI K., LEMSKI P., KOBERDA M., *Validation of Hydraulic Mechanism during Blowout Trauma of Human Orbit Depending on the Method of Load Application*, Appl. Bionics Biomech., 2021, 2021.